Slope Stability Response under Different Rainfall Conditions

Zhe Jin, Haitao Wang

***Abstract*— Slopes are common structures in civil engineering. During rainfall, water infiltration alters soil saturation. This phenomenon threatens the stability of slope materials and increases landslide risk. Thus, a thorough investigation of slope stability under rainfall conditions is essential. Such research is crucial for ensuring engineering safety and environmental protection. This study employs the finite element method to analyze slope stability under various rainfall conditions. The findings can provide a theoretical reference for slope protection against rainfall-induced hazards.**

I. INTRODUCTION

The slope model employs a homogeneous soil. The soil type was selected as cohesive soil from the software's built-in material library. For the seepage analysis conducted in the SEEP/W module, the unsaturated characteristics of the soil must be considered. Consequently, the saturated permeability coefficient and saturated volumetric water content of the soil are required. For the stability analysis performed in the SLOPE/W module, the soil parameters of cohesion, internal friction angle, and unit weight are necessary.

Zhang J et al(2025)Assessing the annual probability of slope failure under these conditions provides critical guidance for landslide risk assessment. Conte E, et al (2022) This study proposes a practical method for predicting shallow landslides triggered by specific rainfall scenarios. Ha N D,et al (2023) Researchers have developed various models and methods for predicting rainfall-induced landslides, which can be broadly categorized into three types: empirical approaches, physics-based models, and machine learning techniques. Zhao B et al (2025) Utilizing methods such as model testing, numerical simulation, and theoretical analysis, this study investigates the mechanisms and prediction of rainfall-induced landslides. The investigation includes the development of monitoring systems, establishment of risk prediction models, and analysis of failure mechanisms. Kang, J.et al (2024) This study utilizes landslide inventories from Yunnan Province, eight predisposing factors, and historical and current rainfall data. The factors include elevation, slope angle, lithology, etc. Crosta G B, Frattini P (2008) . This paper identifies and discusses several key research themes requiring further investigation, such as data uncertainty, the quality of geotechnical analysis, model validation, and the applicability of results within natural hazard frameworks. Wang Het al (2020) This paper examines a representative case where a historical seismic landslide in the northwest loess region was reactivated by rainfall.Brinkgreve R B J. (2005) This study explores the potential and limitations of such models, aiming to provide guidance for selecting appropriate soil models and corresponding parameters for finite element analysis in engineering applications.Derakhshandi M, Pourbagherian H R, Baziar M H, et al (2014) .It demonstrates how long-term monitoring data from construction and operational periods can be used with optimization algorithms to inversely calibrate parameters of complex constitutive models. This represents an advanced level of parameter determination technique.Bagheri F (2022) The 2022 study quantified the impact of climate change on embankment stability by estimating the local factor of safety (LFS) field through coupled stress-seepage finite element analysis. The approach incorporates the concept of suction stress to account for the effect of moisture content on effective stress.Bao X, Cui D, Liao M, et al.(2022)The pore water pressure, saturated zone, and horizontal seepage velocity at different depths within a loess landslide were investigated under various extreme precipitation scenarios.Surjandari N S et al (2019) The analysis quantifies the impact of variations in soil parameters on the slope safety factor. The results of these parameter variations are generalized and processed to derive sensitivity percentages for each parameter relative to the safety factor.

II. MATERIAL AND METHODS (10 BOLD)

2.1 Establishment and Parameterization of the Finite Element Model

A finite element model of the slope was established with corresponding parameters. The slope crest measures 15 m in length. The right slope height is 20 m, and the left height is 10 m. The base length of the slope is 40 m with a gradient of 1:1.5. The influence of groundwater on the seepage field was considered. The left groundwater level is 6 m above the slope toe, and the right level is 8 m above. The mesh was discretized using triangular and quadrilateral elements. The model contains 1,087 nodes and 1,030 elements.

Table 1:

Soil Type	Unit Weight/kg.m-3	Cohesion /kPa	Internal Friction Angle/(°)	Saturated Permeability Coefficient/m.d-1	Saturated Volumetric Water Contnt/(m3/m3)
clay	18.2	12k	23°	0.48	0.32

2.2 Configuration of Boundary Conditions and Monitoring Points

The boundary conditions for the rainfall infiltration model were established based on transient analysis. The slope surface boundary was determined according to rainfall intensity. Considering the groundwater level distribution and

Manuscript received September 28, 2025

Zhe Jin, School of Transportation Engineering, Dalian Jiaotong University, Dalian, China

Haitao Wang, School of Transportation Engineering, Dalian Jiaotong University, Dalian, China

soil permeability, the slope model boundaries were set as follows. The region above the groundwater level was assigned as a zero-flux boundary, representing an impermeable surface. The region below the groundwater level was defined as a head boundary. When rainfall intensity was less than the infiltration capacity of the soil, an infiltration boundary was applied as a flux boundary, with infiltration rate equal to rainfall intensity. When rainfall intensity exceeded the infiltration capacity, a head boundary was used, with the head value determined by the surface elevation. The slope base was treated as an impermeable layer, regarded as a zero-flux boundary, meaning the bottom boundary (gf) was impermeable.

Three characteristic points, A, B, and C, were selected in the slope model at the crest, middle, and toe, respectively. Each point was positioned 1 meter perpendicularly from the slope surface. Additionally, monitoring points D through K were arranged along the crest section at 1-meter intervals.

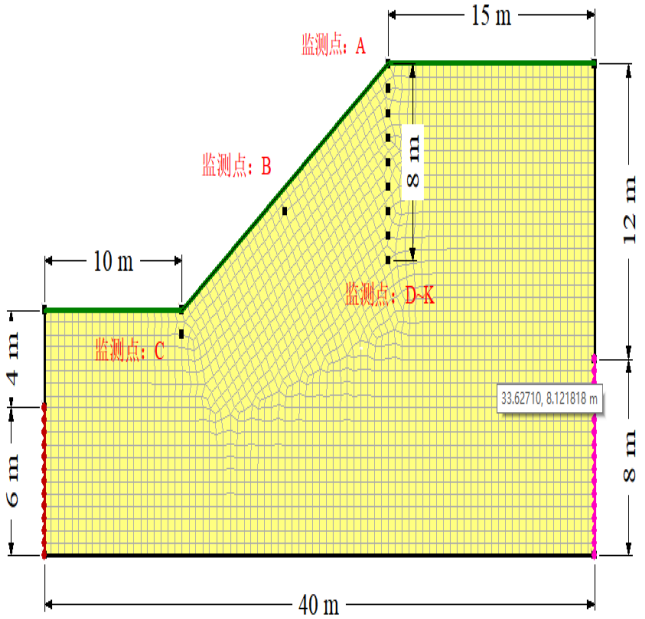

Figure 1: Schematic of the Model Mesh

2.3 Analysis of Initial Slope Conditions

First, a steady-state analysis was conducted using the SEEP/W module to determine the initial pore water pressure distribution within the slope model. This distribution served as the initial condition for analyzing various rainfall intensities, patterns, and durations. Subsequently, a transient analysis was performed based on this initial state to investigate pore water pressure variations under different influencing factors. The steady-state results are time-independent. The transient analysis spanned 36 hours, with the first 24 hours simulating rainfall application and the subsequent 12 hours monitoring the response after rainfall cessation. The dashed line in the figure indicates the phreatic line, representing the groundwater table under steady-state conditions. The pore water pressure at this line is 0 kPa. Above the phreatic line, pore water pressures are negative, indicating an unsaturated zone. This zone contributes to slope stability. Pore water pressure decreases linearly with increasing slope height. The initial seepage field results were imported into the SLOPE/W module, and the limit equilibrium method was applied. The initial safety factor of the slope was calculated as 1.915, as shown in Figure 3.

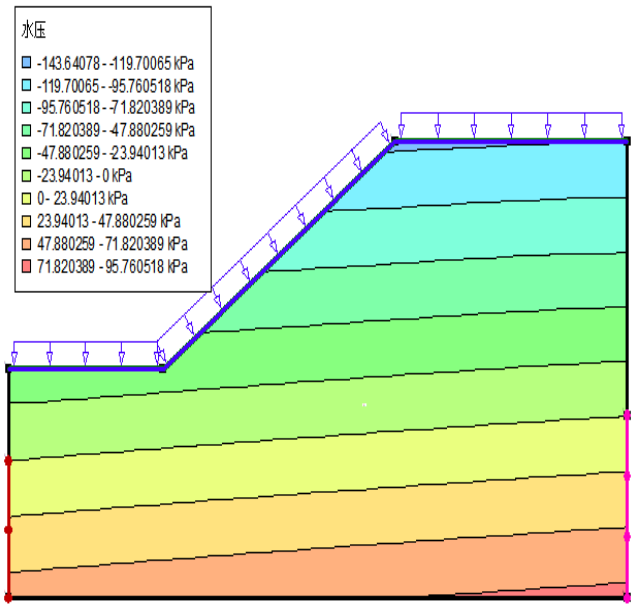

Figure 2: Distribution of Initial Pore Water Pressure

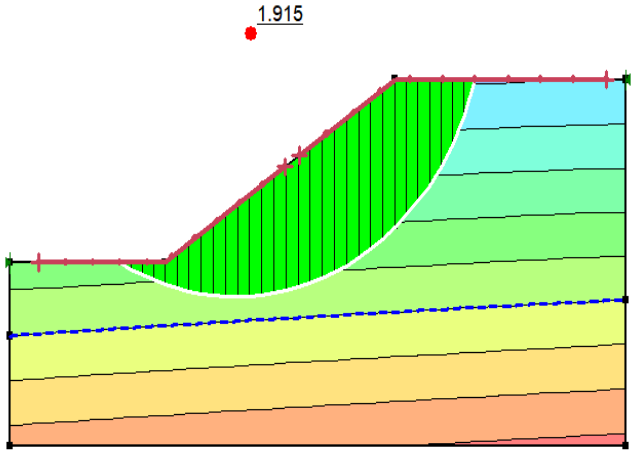

Figure 3: Initial Safety Factor

2.4 Contour Plots of Pore Water Pressure after Rainfall

Simulations were conducted using a uniform rainfall pattern. The rainfall intensities included moderate rain (24 mm/d), heavy rain (48 mm/d), and storm rain (96 mm/d). The variations in pore water pressure and safety factor were analyzed over a 36-hour period. This period comprised 24 hours of rainfall followed by 12 hours of post-rainfall monitoring.

Three rainfall intensities were applied to the slope model surface via the SEEP/W module. The simulation results captured the pore water pressure response during the 24-hour rainfall event.

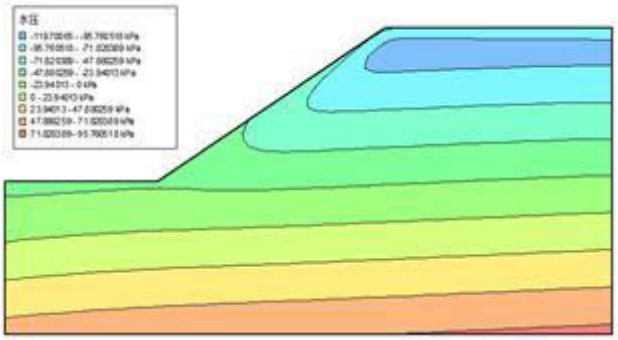

Moderate Rain Condition

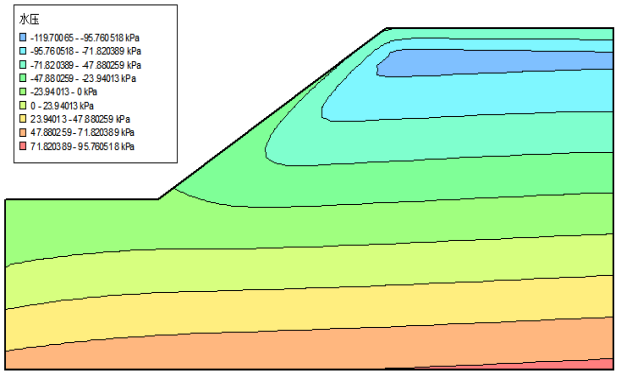

Heavy Rain Condition

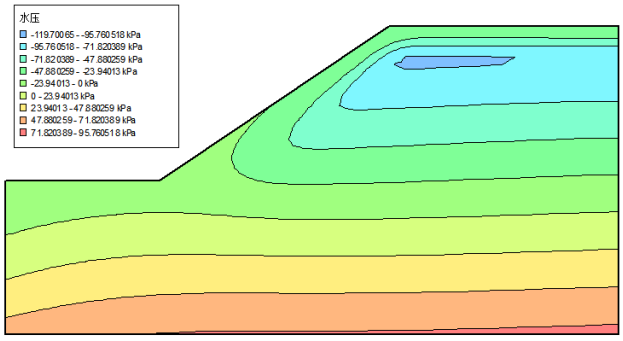

Storm Condition

Figure 4: Comparison of Pore Water Pressure Contours after 24-hour Rainfall

Under the same rainfall duration, different rainfall intensities exert varying degrees of influence on slope pore water pressure. Pore water pressure changes with increasing rainfall intensity. At the slope crest, higher rainfall intensity leads to more pronounced pore water pressure responses in the surface soil. Specifically, increased rainfall intensity raises pore water pressure at the crest, thereby reducing matric suction. Similar trends are observed at the slope face and toe.

Pore water pressure contours at the end of rainfall do not clearly reflect the rate of change during the rainfall period. Thus, characteristic point A at the crest was selected as an observation section to analyze the variation of pore water pressure with time at different elevations. Figure 5 shows the curves of pore water pressure versus time at different heights along the crest section under three rainfall intensities.

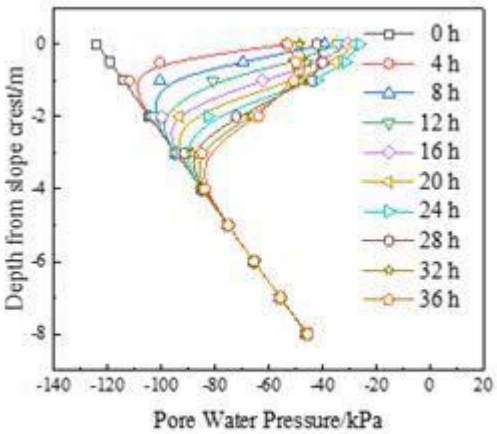

Moderate Rain Condition

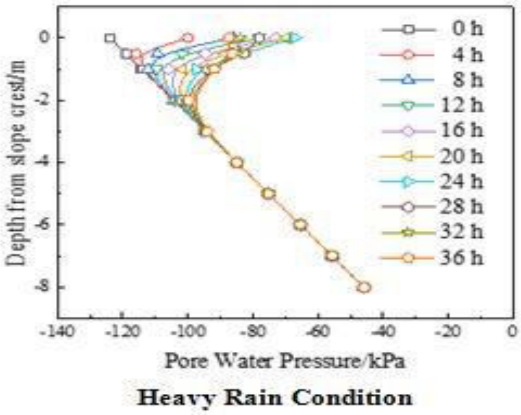

Heavy Rain Condition

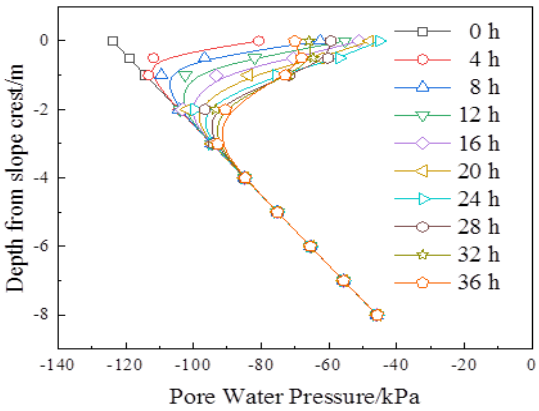

Storm Condition

Figure 5: Time-Variation of Pore Water Pressure at Varying Elevations

The curves of pore water pressure versus slope height at different times indicate that the rainwater infiltration depth increases with rainfall duration. Under all rainfall intensities, the wetting front moves downward as rainfall progresses. After rainfall ceases, the wetting front rises due to pore water pressure dissipation. The influence of rainfall intensity on infiltration depth varies. This section investigates the influence of different rainfall intensities on the pore water pressure at characteristic points within the same duration, aiming to quantify the impact of rainfall intensity at various slope locations. Figure X presents the pore water pressure at three characteristic points—slope crest (A), slope surface (B), and slope toe (C)—after 24 hours of rainfall under different intensity levels.

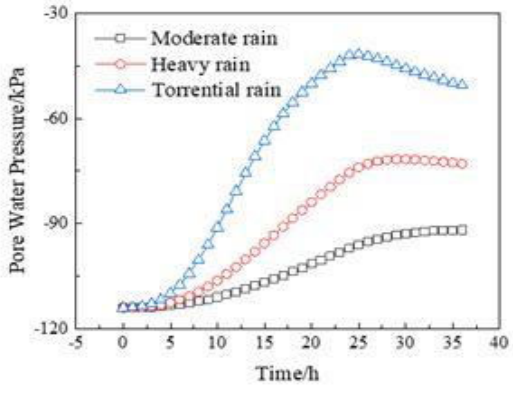

A

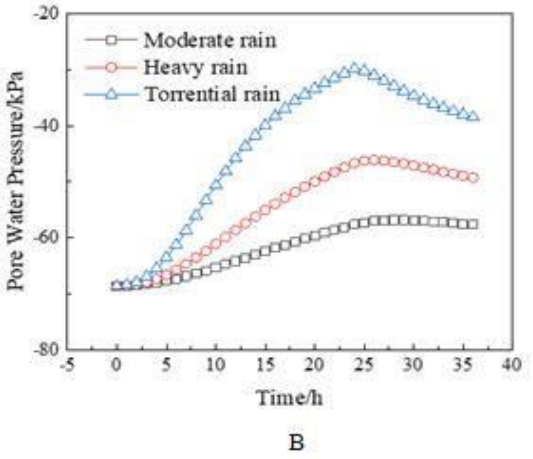

B

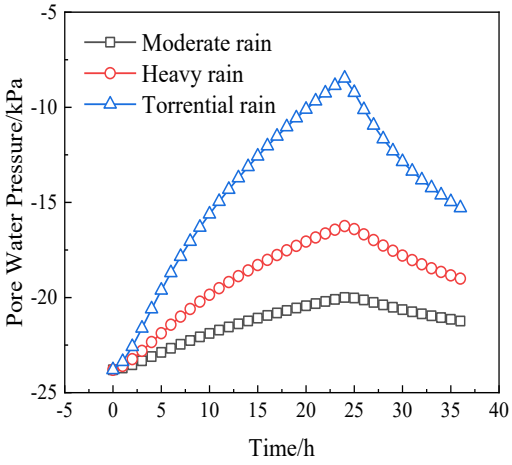

C

Figure 6

Under uniform rainfall patterns, pore water pressure near the slope top, middle, and bottom surfaces changes differently as rainfall continues. Higher rainfall intensity leads to greater variation amplitudes in pore water pressure at these characteristic points. After rainfall ceases, the pore water pressure gradually dissipates. For the same rainfall duration, the degree of pore water pressure change varies with rainfall intensity. The pore water pressure in the soil near the slope top is more sensitive to rainfall intensity, showing a significant increase in variation amplitude under heavier rainfall. Thus, when the rainfall pattern remains constant, rainfall intensity has a relatively stronger influence on pore water pressure changes at the slope top, while its effect is weaker at the slope bottom. Under the same rainfall intensity, the slope top exhibits the largest variation amplitude, followed by the slope middle, and the slope bottom shows the smallest change. Moreover, the increasing rate of pore water pressure rises with rainfall intensity, being the smallest during moderate rain, intermediate during heavy rain, and the largest during storm rain.

2.5 Time-History Curves of Slope Safety Factors

To analyze the influence of rainfall intensity on slope stability, three levels—moderate rain, heavy rain, and storm rain—were applied to the slope surface. Figure illustrates the variation of the slope safety factor over time under these different rainfall intensities.

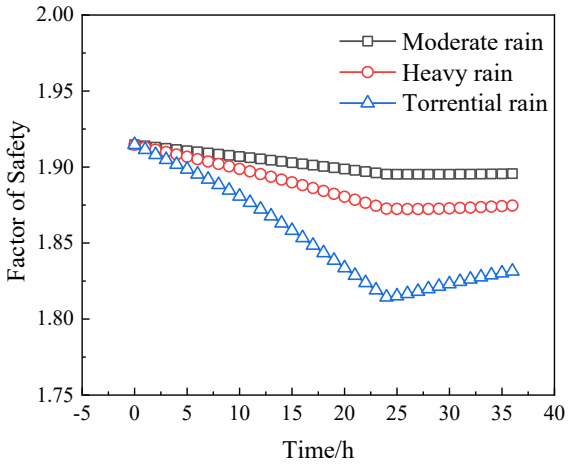

Figure 7: Evolution of Slope Safety Factor with Rainfall Pattern and Time

Under the three rainfall levels, the slope safety factor gradually decreased with ongoing rainfall. A higher rainfall intensity led to a greater reduction in the safety factor. This is because more intense rainfall results in a larger volume of water infiltration per unit time, which causes more significant changes in pore water pressure within the slope. Changes in pore water pressure alter the soil matric suction, directly affecting the soil's shear strength. Concurrently, the increase in soil saturation leads to a higher soil unit weight. The combined effect of these factors results in a pronounced decrease in the safety factor. Within 12 hours after rainfall ceased, the safety factor recovered. The magnitude of this recovery was positively correlated with the previous rainfall intensity. This phenomenon is attributed to the dissipation of pore water pressure after rainfall.

DISCUSSION AND CONCLUSION

The effects of three rainfall intensities—moderate rain (24 mm/d), heavy rain (48 mm/d), and storm rain (96 mm/d)—on the slope seepage field were simulated. The results indicate that higher rainfall intensity leads to a greater variation in pore water pressure. Under different rainfall conditions, the response of pore water pressure varies across slope regions. The most pronounced change occurs at the crest, followed by the slope face, while the toe shows the least variation. Furthermore, increased rainfall intensity results in a notable decrease in the safety factor, thereby reducing slope stability.

REFERENCES

[1]. Zhang J, Yang B, Lu M, et al. Assessing annual failure probability of soil slopes under rainfall and evaporation[J]. Computers and Geotechnics, 2025, 187: 107517.

[2]. Conte E, Pugliese L, Troncone A. A simple method for predicting rainfall-induced shallow landslides[J]. Journal of Geotechnical and Geoenvironmental Engineering, 2022, 148(10): 04022079.

[3]. Ha N D, Duong N H. Advancements, Challenges, and Future Directions in Rainfall-Induced Landslide Prediction: A Comprehensive Review[J]. Journal of Engineering & Technological Sciences, 2023, 55(4).

[4]. Zhao B, Marin R J, Luo W, et al. Rainfall thresholds for shallow landslides considering rainfall temporal patterns[J]. Bulletin of Engineering Geology and the Environment, 2025, 84(3): 1-13.

[5]. Kang, J., Wan, B., Gao, Z. et al. Research on machine learning forecasting and early warning model for rainfall-induced landslides in Yunnan province. Sci Rep 14, 14049 (2024).

[6]. Crosta G B, Frattini P. Rainfall-induced landslides and debris flows[J]. Hydrological Processes: An International Journal, 2008, 22(4): 473-477.
[7]. Wang H, Sun P, Zhang S, et al. Rainfall-induced landslide in loess area, Northwest China: a case study of the Changhe landslide on September 14, 2019, in Gansu Province[J]. Landslides, 2020, 17(9): 2145-2160.
[8]. Brinkgreve R B J. Selection of soil models and parameters for geotechnical engineering application[M]//Soil constitutive models: Evaluation, selection, and calibration. 2005: 69-98.
[9]. Derakhshandi M, Pourbagherian H R, Baziar M H, et al. Numerical analysis and monitoring of a rockfill dam at the end of construction (case study: Vanyar dam)[J]. International Journal of Civil Engineering, 2014, 12(4): 326-337.
[10]. Bagheri F. Effect of Climate Change on Slope Stability of Variably Saturated Embankments Using Local Factor of Safety and In-Situ Stress Finite Element Analysis[J]. 2022
[11]. Bao X, Cui D, Liao M, et al. Analysis of the formation mechanism of rainfall-induced loess landslide: A case study of Beiyin landslide[J]. 2022.
[12]. Surjandari N S, Riyadinata F D, Purwana Y M. Sensitivity analysis of soil parameters on slope stability using simplified Bishop method (case study in Grobogan, Central Java, Indonesia)[C]//Journal of Physics: Conference Series. IOP Publishing, 2019, 1376(1): 012012.